# Primary measurement method for the characterisation of impedance standard in the mΩ range

OPEN ACCESS
IOP Publishing
Measurement Science and Technology
Meas. Sci. Technol. **33** (2022) 085016 (11pp)
https://doi.org/10.1088/1361-6501/ac6a45

# Primary measurement method for the characterisation of impedance standard in the mΩ range

**Benyamin H Rusanto**[1], **Steffen Seitz**[1,*], **Torsten Funck**[2] **and Marco Heinrich**[1]

[1] Department 3.13 Electrochemistry, Physikalisch- Technische Bundesanstalt-PTB, Braunschweig, Germany
[2] Department 2.13 AC-DC Transfer, impedance, Physikalisch- Technische Bundesanstalt-PTB, Braunschweig, Germany

E-mail: steffen.seitz@ptb.de

Received 9 January 2022, revised 21 April 2022
Accepted for publication 25 April 2022
Published 18 May 2022

**Abstract**

Impedance standards having impedance values in the low mΩ range, with non-zero reactances, and operable with alternating current-currents of a few Amps and up to a few kHz are needed for appropriate impedance meter calibration. These challenging operation parameters are most relevant for electrochemical impedance spectroscopy of high energy Li-ion battery cells. We present a primary measurement method that can be used for the characterisation of respective impedance standards traceable to the SI. Basically, two calibrated high precision DC voltage meters are used to sample the voltages across a characterised reference resistor and the impedance standard under test, while both are excited with the same ac current. The measured voltages are fitted with sin waves and the complex impedance value is calculated from the amplitudes and phase difference of the voltage curves. We present the measurement results of a test impedance in mΩ range, including a full uncertainty budget. Moduli of the measured impedances are compared with those of another method that has been presented recently. The results are equivalent up to 1 kHz and within a relative expanded uncertainty of around 0.47%.

Keywords: low impedance, impedance standard, primary measurement method, uncertainty, comparison

(Some figures may appear in colour only in the online journal)

## 1. Introduction

Electrochemical impedance spectroscopy (EIS) is often used to characterize the performance of Li-ion battery (LIB) cells [1]. LIB cells used in electromobility applications usually have low impedance values in the mΩ range and below. Currently, there are no impedance standards available the assigned values of which are traceable to the International System of Units (SI). As a consequence, the metrological comparability [2] of results measured with different impedance meters is questionable in this range. Moreover, impedances of LIB cells usually show significant reactances, while calibration is usually performed only with resistors, ignoring varying phase angles. These shortcomings in the calibration of impedance spectrometers introduce significant uncertainties to the measured impedances [3]. Therefore, establishing traceability of impedance measurements results to the SI through well characterised impedance standards is a prerequisite for accurate impedance measurements of LIBs.

* Author to whom any correspondence should be addressed.



 

In order to improve traceability of impedance results in the full complex plane, a few impedance bridges and impedance standards have recently been developed [4–7]. Results of comparison of electrical impedance standards have recently been reported in the framework of the AIMQute project [8]. That comparison, which is the first of its kind, involves a standard impedance angle with a phase angle of ±30° and ±60° and, and a magnitude ranging from about 100 Ω to 1 MΩ. An automated impedance simulator, called iSimulator, which is capable of simulating the impedance of an impedance standard [9] has been developed to calibrate LCR-meters over the full complex plane in the frequency range from 50 Hz to 20 kHz and in the impedance range from 1 Ω to 10 MΩ. Impedance measurements of an RC element in series to a resistor have been demonstrated in the mΩ range and in a frequency range up to 10 kHz using effective voltage and current measurements [10] that are traceable to the SI. That technique however can only be used in conjunction with this specific circuitry, assuming negligible interfering impedances [11]. Some progress is currently made within the EMPIR project 'LiBforSecUse' to develop and establish low impedance standards [3], which fit well into the scope this work.

We demonstrate a primary measurement set-up that can be used to measure impedances with arbitrary phase angles, in the range of a few mΩ, frequencies up to 1 kHz, and with currents of a few amperes, which are the operation parameters typically needed for EIS of LIBs. Basically, the set-up consists of two synchronised, high precision digital voltmeters and a high precision, low-inductance alternating current (AC)-resistor. The voltmeters, the resistor and the external trigger used for the synchronisation are each calibrated traceable to the SI. Thus, the measured impedances are likewise traceable to the SI. We will further provide a full uncertainty budged of the measurement results aiming at a target of 1% relative standard uncertainty. This target uncertainty is sufficient for impedance-based charcterisation of LIBs, since uncertainties introduced by the battery are assumed to be significantly larger [1]. However, impedance standards (e.g. current shunts or reactance standards) and their characterisation might strive for smaller uncertainties [11].

In a first section we will describe the measurement set-up. In the second section we will discuss the uncertainty contributions to the measurement. Finally, we demonstrate the results of an impedance measurement of an RC element and compare them with the results of a measurement using the method of [10].

## 2. Reference spectrometer or low impedance measurements

### 2.1. Electrical impedance

The electrical impedance extends the concept of an ohmic resistance to AC circuits, describing not only the relation between the voltage and current amplitudes, but also their phase difference [12]. Therefore, if a sinusoidal voltage $v(t)$ is applied to a passive, electric element or circuit, thereby generating a linear current response $i(t)$, or vice versa, the impedance $Z$ is expressed as the ratio of both electric signals:

$$v(t) = V\cos(2\pi ft + \varphi_v) = \text{Real}\left(Ve^{j2\pi ft}e^{j\varphi v}\right) \quad (1)$$

$$i(t) = I\cos(2\pi ft + \varphi_i) = \text{Real}\left(Ie^{j2\pi ft}e^{j\varphi_i}\right). \quad (2)$$

$V$ and $I$ are the voltage and current amplitudes, $\varphi_v$ and $\varphi_i$ are the respective phases, $j$ is the imaginary unit, and $f$ is the frequency. AC voltages and currents are usually denoted as complex phasors, basically omitting the frequency dependency:

$$\bar{I} = Ie^{j\varphi_i} \quad (3)$$

$$\bar{V} = Ve^{j\varphi_v}. \quad (4)$$

Thus, the impedance is given as:

$$Z = \frac{\bar{V}}{\bar{I}} = \frac{V}{I}e^{j(\varphi_v-\varphi_i)} = \frac{V}{I}e^{j\varphi} = |Z|\cdot e^{j\varphi}$$
$$= |Z|\cdot\cos(\varphi) + j|Z|\cdot\sin(\varphi) = Z' + jZ''. \quad (5)$$

Equation (5) also denotes various representations of $Z$ that are often used. $|Z|$ is the modulus of the impedance and $\varphi = \varphi_v - \varphi_i$ is the phase difference between the voltage and the current. Note that $|Z|$ and $\varphi$ depend on frequency, since the linear frequency response of the current, i.e. its amplitude and phase, to an impressed voltage (and vice versa) depends on frequency. It must be emphasized that linearity between the excitation signal and the response is a fundamental prerequisite for the impedance concept. Electrochemical systems, i.e. LIBs, are actually non-linear. However, provided the amplitude of the excitation signal is small enough, which should be experimentally verified, they can be approximately considered linear. LIBs are designed to have small internal resistances to minimize thermal power loss. High energy cells with capacities of up to some tens of Ah have impedances in the low mΩ range and below. The frequency ranges related to the time constants of the most relevant electrochemical processes reach from the low mHz range up to some kHz, depending on the electrochemical and geometrical properties of the cell [1].

### 2.2. Basic concept of the impedance measurement set-up

The basic concept of the impedance measurement set-up is outlined in figure 1. It consists of two high precisions digital multimeters (DMM), a high precision reference resistor, an external trigger and a programmable current generator.

A sin-wave current $i_m(t)$ is impressed on the reference resistor (Precision AC Current Shunt Fluke A40B) and the device under test (DUT). The reference resistor is a high precision, coaxial current shunt to minimize inductive interference [13]. The wires connecting the current source to the resistor and the DUT are twisted as good as possible to minimize measurement errors through inductive coupling. The voltages are measured in 4T (four terminal) setups.

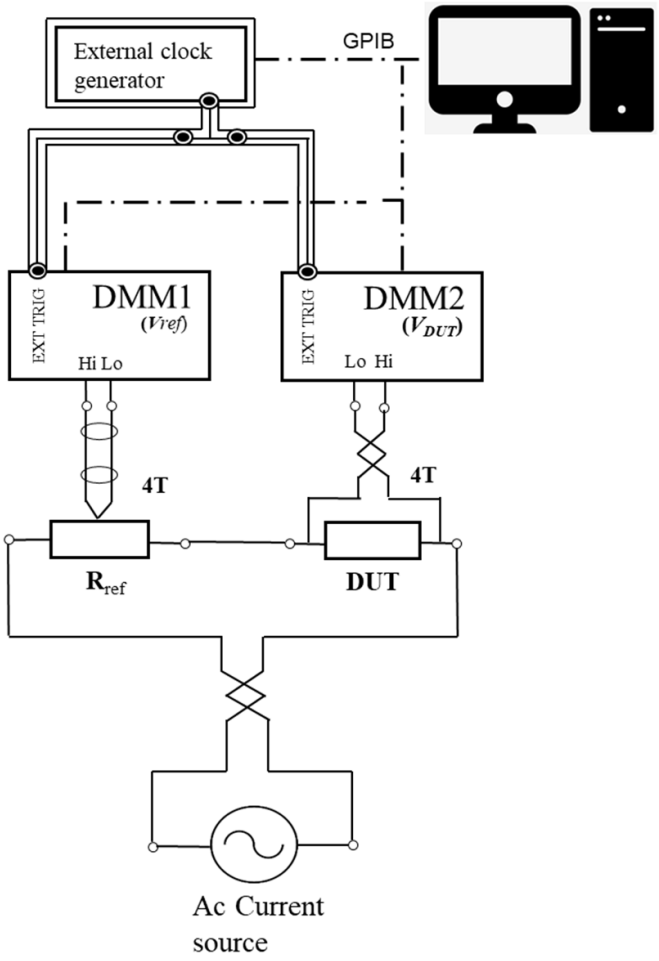


**Figure 1.** Outline of the spectrometer set-up for impedance measurement.

$i_m(t)$ is measured by the voltage drop $v_{ref}(t)$ across the reference resistor with a Keysight 3458A (DMM1), which provides appropriate accuracy for the sampling of low-frequency voltages [14–16]:

$$i_m(t) = \frac{v_{ref}(t)}{R_{ref}}. \tag{6}$$

$R_{ref}$ is the DC value of the reference resistor. The sin-wave current is generated using a programmable generator and a linear amplifier. The voltage drop $v_{DUT}(t)$ across the device under test (DUT) is measured with a second Keysight 3458A (DMM2). An external trigger Keysight 33500 pulse generator is used to trigger both DMMs to synchronize the time axis of both measurements. The time axis is given by the trigger frequency. The signal amplitudes $V_{ref}$, $V_{DUT}$ and the phase difference $\varphi$ are subsequently determined by fitting sine curves into the measured voltage data. Using equation (5) the impedance $Z_{DUT}$ of the DUT is then calculated from:

$$Z_{DUT} = \frac{V_{DUT} R_{ref}}{V_{ref}} e^{j\varphi}. \tag{7}$$

### 2.3. Traceability of the measured impedance

Only if measurement results are linked to a common reference, preferably the SI, through a documented unbroken calibration chain, meaning they are 'traceable' to that reference, their quantity values are measured on the same scale. Only such measurement results can reasonably be compared with each other, meaning they are 'metrologically comparable' [2].

Fundamentally, all impedance spectrometers measure the voltage and the current signals applied to the DUT, and their phase difference, even though the technical realisation can be quite different. In any case, traceability of the individual quantities cannot easily be accomplished with commercial impedance meters since they are not accessible for the user. Therefore, such spectrometers must be calibrated with adequate impedance standards, the impedance values of which must be determined by other means.

This can be achieved with the spectrometer described above. Looking at equation (7) it is obvious that the four input quantities $V_{ref}$, $V_{DUT}$, $R_{ref}$ and $\varphi$ measured with our set-up must be linked to SI standards to establish SI traceability for impedance measurements. These quantities are measured independently. Thus, SI traceability of the impedance $Z_{DUT}$ can easily be established through the calibration of the individual measurement devices with respect to SI voltage, resistance and, regarding measurement frequency, time standards. These calibrations have been conducted at the respective departments of the national metrology institute of Germany, the Physikalisch-Technische Bundesanstalt (PTB).

### 2.4. Measurement procedure and parameters

Data acquisition and processing algorithms applied to obtain the measurement results have been implemented in LabView. The sampling mode to measure $v_{ref}(t)$ and $v_{DUT}(t)$ was set to the DCV mode of the DMMs to digitize the sinusoidal voltages. The amplitude of the current generator was set to about 2 A so that the voltage amplitude $V_{ref}$ at the reference resistor (80 mΩ) was about 160 mV. The sine wave frequencies ranged from about 1 Hz to 3 kHz with ten logarithmic steps per decade.

The measurement of the sinusoidal signal by a DMM at a given frequency is illustrated in figure 2. Each individual voltage measuring point was started by an external trigger. The voltage was then measured for an integration time $t_{int}$. In DCV mode, the integration time can be set by the user. Due to technical limitations the resolution of the A/D converter is determined by the integration time, which, in turn, determines the maximal sampling trigger frequency and vice versa. We have calculated the optimal integration times according to:

$$t_{int} = 0.9342 t_s - 9\ \mu s \tag{8}$$

from the specifications of the manufacturer. $t_s$ is described below.

The DMM has continuously been triggered with the set trigger frequency $f_{trig}$ until a number $N$ of trigger-pulses have been applied to obtain $N$ voltage measurements of the sine signal.

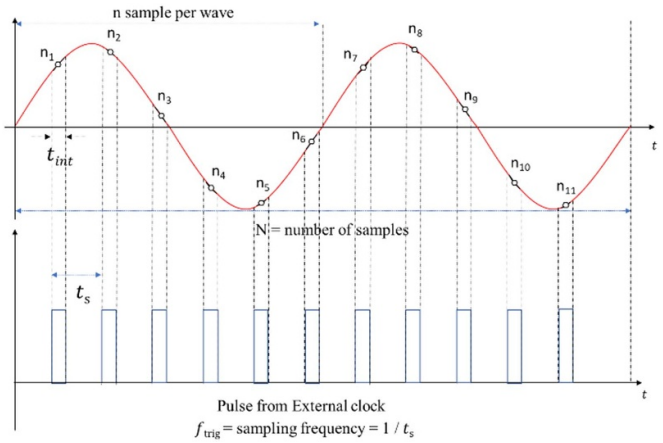


**Figure 2.** The measurement of the sinusoidal signal by a DMM.

These $N$ voltage measurements define a sweep. Thus, a sweep may include the measurement of several sine waves, depending on the set values for $N$ and $f_{\text{trig}}$. The sampling time $t_s$ is defined by the time between two samplings, i.e. $t_s = 1/f_{\text{trig}}$. The number of samples per sine wave at a given frequency, was limited by the sampling capability of the DMMs. To achieve reasonable fits of the sine curves, we have set a lower limit of 16 samples per sine wave. Thus, the smallest sampling time is about 19 µs for a 3 kHz sine wave. The time axis was realized by the calibrated pulse generator. The voltage data have been stored in the internal memory of the DMM during the measurement. After a sweep, they have been retrieved with LabView. Each trigger pulse has been applied to both DMMs to synchronize the time axes of the measurements of both voltage signals.

### 2.5. Data processing

The Levenberg–Marquardt algorithm was applied to fit the sampling data of the sinusoidal voltages. The measured sinwaves can be described as:

$$v_{\text{fit\_ref}}(t) = A_{\text{ref}} \cos(2\pi B_{\text{ref}} t + C_{\text{ref}}) + D_{\text{ref}} \tag{9a}$$

$$v_{\text{fit\_DUT}}(t) = A_{\text{DUT}} \cos(2\pi B_{\text{DUT}} t + C_{\text{DUT}}) + D_{\text{DUT}}. \tag{9b}$$

Thus, the fitting was conducted by a four-parameter, nonlinear curve fitting algorithm to the measured data sets $(t_i, v_{\text{ref}}(t_i))$ and $(t_i, v_{\text{DUT}}(t_i))$, respectively, according to the IEEE Standard 1057-2017 [17]. $V_{\text{ref\_fit}}$, $f_{\text{ref\_fit}}$ and $\varphi_{\text{ref\_fit}}$ are calculated from $A_{\text{ref}}$, $B_{\text{ref}}$, $C_{\text{ref}}$, and $D_{\text{ref}}$. $V_{\text{DUT\_fit}}$, $f_{\text{DUT\_fit}}$ and $\varphi_{\text{DUT\_fit}}$ are calculated from $A_{\text{DUT}}$, $B_{\text{DUT}}$, $C_{\text{DUT}}$ and $D_{\text{DUT}}$.

The measurement procedure includes a number of uncertainties to be considered. They will be discussed in the next section.

## 3. Measurement uncertainties

The measurement uncertainty of $Z_{\text{DUT}}$ is calculated according to GUM [18]. The uncertainty budget is based on equation (7). Thus, the main sources of uncertainty to the input quantities,

- amplitude of the sin-voltages of the reference resistor $V_{\text{ref}}$,
- amplitude of the sin-voltages of the DUT $V_{\text{DUT}}$,
- phase difference φ between both sin-voltages,
- value of the reference resistor, $R_{\text{ref}}$,

must be investigated. In the following, we will discuss the uncertainty contributions to each input quantity step by step.

### 3.1. Amplitudes $V_{ref}$ and $V_{DUT}$

*3.1.1. Calibration of DMM.* The DMMs have been calibrated at PTB. Calibration results of DMM1 and DMM2 are shown in table 1, which indicate the deviation $\Delta V_{\text{cal}}$ (third column) from the reference value (second column) and the expanded uncertainty of the deviation $U(\Delta V_{\text{cal}})$ (forth column). We have corrected the amplitudes $V_{\text{ref\_fit}}$ and $V_{\text{DUT\_fit}}$ for the deviation, applying:

$$V_{\text{ref}} = V_{\text{ref\_fit}} - \Delta V_{\text{cal}} \tag{10a}$$

$$u^2(V_{\text{ref}}) = u^2(V_{\text{ref\_fit}}) + u(\Delta V_{\text{cal}})^2. \tag{10b}$$

The correction of $V_{\text{DUT\_fit}}$ and its uncertainty is calculated accordingly.

*3.1.2. Long term instability.* The uncertainty $u_{\text{ls}}$ of the voltage measurement increases over time due to a small unpredictable drift of the instrument. Table 2 quantifies the effect. The values are determined from [19]. The time refers to the period $t$ elapsed after last calibration. $U_z$ (in table 2) is the voltage reference value. We have assumed a linear dependence on time to estimate this uncertainty contribution.

$$u_{\text{ls}}(t, \text{ in range } U_z) = a(\text{in range } U_z)\, t + \text{Const}(\text{in range } U_z) \tag{11}$$

where $a$ and Const have been calculated from a linear interpolation of the values given in table 2.

*3.1.3. Gain error.* As mentioned, the maximal sampling frequency, $f_{\text{trig}}(\text{max})$, depends on the integration time and on the resolution of the A/D converter of the DMM and affects the gain error. Thus, the uncertainty budget must consider the gain error, depending on the selected settings. Table 3 shows the correlation [20].

*3.1.4. Fitting uncertainty.* The uncertainty of the fit, $u_{\text{fit}}$, is represented by the residuals of the fit calculated by the mean

**Table 1.** Results from DMM 1 and 2 (3458 A DCV) calibration certificate with expanded Unc ($k = 2$).

| Reference voltage | Measured value | Deviation $\Delta V_{\text{cal}}$ | uncertainty $u(\Delta V_{\text{cal}})$ |
|---|---|---|---|
| DMM 1 set range 1 V | | | |
| 0.100 000 V | 0.099 9998 V | −0.000 0002 V | 1.4 μV |
| DMM 2 set range 100 mV | | | |
| 10.000 000 mV | 9.998 55 mV | −0.001 45 mV | 0.73 μV |

**Table 2.** Values used to estimate the uncertainty contribution due to long term instability.

| Range/$U_z$ | Basic accuracy | | | |
|---|---|---|---|---|
| | 90 d $\mu V^{-1}$ | | 1 year $\mu V^{-1}$ | |
| | $a$ | Const | $a$ | Const |
| 100 mV | 5.0 | 3.0 | 9.0 | 3.0 |
| 1 V | 4.6 | 0.3 | 8.0 | 0.3 |

**Table 3.** Gain error and its dependence on the resolution of A/D converter, maximum sampling frequency and integration time.

| Integration time $t_{\text{int}}$/ms | Resolution of A/D converter/bits | Maximum sampling frequency $f_{\text{trig}}$ (max)/Hz | Gain error /ppm |
|---|---|---|---|
| 0.012 | 18 | 41 666 | 30 |
| 0.2 | 21 | 4416 | 16 |
| 2 | 21 | 493 | 2.2 |
| 20 | 25 | 50 | 0.5 |

square error (MSE) between the best nonlinear fit and the sampling data:

$$u_{\text{fit}}^2 = \text{MSE} = \frac{1}{N}\sum_{i=1}^{N}(v_i - v_{\text{fit}})^2. \tag{12}$$

$v_i$ is the measured value $v(t_i)$ at the time $t_i$ and $v_{\text{fit}}$ is the corresponding value of the fitted sin voltage function according to equation (9). The uncertainty results mainly from noise present in the measured voltages and spurious components which might be present in the input signal [17]. Figure 3 shows exemplarily the moduli of the residuals for a measurement of a 100 Hz voltage signal of a test impedance (resistance in series to an RC element, see section 4.1), measured with both DMMs. The test impedance was in the order of 1 mΩ and the applied current was around 2 A. There is a small dependence of the residuals on voltage that can be seen from the sinusoidal (≈250 Hz) like shape of the residuals. Its origine could not be identified.

Table 4 shows quantity values of $u_{\text{fit}}$ exemplarily at some frequencies for the voltage amplitudes of the reference resistor ($V_{\text{ref}}$) and of the test impedance ($V_{\text{DUT}}$) mentioned above. The uncertainty increases slightly with frequency for the reference resistor but shows no significant dependence on frequency for the DUT.

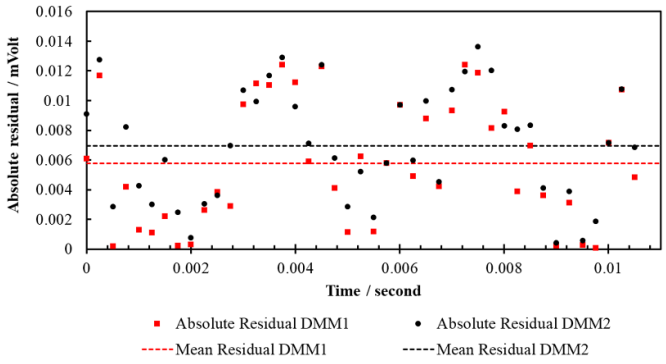


**Figure 3.** Absolute residual between sampling data and fitting for DMM1 and DMM2.

**Table 4.** Exemplary fitting uncertainty for a test impedance.

| Freq/Hz | $V_{\text{ref}}$/mV | $V_{\text{DUT}}$/mV | $u_{\text{fit}}(V_{\text{ref}})$/mV | $u_{\text{fit}}(V_{\text{DUT}})$/mV |
|---|---|---|---|---|
| 3162 | 185.12 | 5.246 | 0.12 | 0.011 |
| 1000 | 190.77 | 3.556 | 0.11 | 0.007 |
| 100 | 192.46 | 3.249 | 0.07 | 0.004 |
| 10 | 192.14 | 6.559 | 0.05 | 0.003 |
| 1 | 193.42 | 7.347 | 0.03 | 0.001 |

Table 5 summarizes the uncertainty contributions exemplarily for the voltage amplitudes of the test impedance according to section 4.1 at 100 Hz. The major contributions result from fitting the signals. The overall combined standard uncertainty of the voltage amplitude is 2.2 μV.

Table 6 indicates the combined uncertainties for the amplitudes of the reference resistor and the DUT for various frequencies. The uncertainties increase slightly with frequency.

### 3.2. *Phase difference* φ

The main uncertainty contributions to the phase difference are:

(a) fitting of $v_{\text{ref}}$ $(t)$ and $v_{\text{DUT}}$ $(t)$.
(b) synchronisation error.

*3.2.1. Fitting.* The uncertainty of the fitting not only effects the voltage amplitude as described above, but also the derived phase difference. To estimate the uncertainty contribution for the phases of $v_{\text{ref}}$ $(t)$ and $v_{\text{DUT}}$ $(t)$ we have measured seven sweeps for each voltage signal and calculated the standard deviation of the phases derived from fits to each sweep. Since this procedure is quite time consuming, it has been conducted only once and this uncertainty contribution has been assigned to each subsequent measurement. The results are shown in table 7 for various frequencies.

*3.2.2. Synchronisation.* Synchronisation of the DMM devices is required to assign the same time axis to both voltage

**Table 5.** Uncertainty budget of voltage amplitude measurements at 100 Hz.

| Description | $u_{nc}$ | PD | div | $c_i$ | $u_{std}$ |
|---|---|---|---|---|---|
| Calibration of DMM2 | $7.3 \times 10^{-7}$ V | $N$ | 2 | 1 | $3.7 \times 10^{-7}$ V |
| Long term instability | $3.3 \times 10^{-7}$ V | $R$ | $\sqrt{3}$ | 1 | $1.9 \times 10^{-7}$ V |
| Gain error | $5.2 \times 10^{-8}$ V | $R$ | $\sqrt{3}$ | 1 | $3.0 \times 10^{-8}$ V |
| Fitting | $4.4 \times 10^{-6}$ V | $N$ | 2 | 1 | $2.2 \times 10^{-6}$ V |
| Combined uncertainty | | | | | $2.2 \times 10^{-6}$ V |

$u_{nc}$ = Uncertainty range
PD = Probability distribution ($N$ = Normal; $R$ = Rectangular)
div = Divisor
$c_i$ = Sensitivity coefficient
$u_{std}$ = Contribution to the standard uncertainty

**Table 6.** Combined uncertainty for the amplitude of the reference resistor and DUT at some frequencies.

| Freq/Hz | $V_{ref}$/mV | $u(V_{ref})$/mV | $V_{DUT}$/mV | $u(V_{DUT})$/mV |
|---|---|---|---|---|
| 3162 | 185.12 | 0.062 | 5.246 | 0.005 |
| 1000 | 190.77 | 0.055 | 3.556 | 0.003 |
| 100 | 192.46 | 0.034 | 3.249 | 0.002 |
| 10 | 192.14 | 0.024 | 6.559 | 0.001 |
| 1 | 193.42 | 0.014 | 7.347 | 0.001 |

**Table 7.** Uncertainty of the phase difference due to fitting uncertainties.

| Freq/Hz | Phase difference $\varphi$/° | $u(\varphi_{fit})$/° |
|---|---|---|
| 3162 | 42.790 | 0.046 |
| 999 | 22.326 | 0.022 |
| 100 | −10.708 | 0.0073 |
| 10 | −15.551 | 0.0036 |
| 1 | −1.858 | 0.00019 |

**Table 8.** Synchronize test results. The values indicate the relative phase difference between measurements with both DMMs.

| Freq/Hz | Test impedance | $R_{ref}$ | $u_{sync}$ |
|---|---|---|---|
| 1000 | 0.023% | 0.041% | 0.041% |
| 100 | 0.024% | 0.025% | 0.025% |
| 10 | 0.0005% | 0.023% | 0.023% |
| 1 | 0.0002% | 0.0065% | 0.0065% |

**Table 9.** Uncertainty budget of phase measurement at 100 Hz.

| Description | $u_{nc}$/° | PD | div | $c_i$ | $u_{std}$/° |
|---|---|---|---|---|---|
| Fitting $v_{DUT}(t)$ | $3.8 \times 10^{-3}$ | $N$ | 2 | 1 | $1.90 \times 10^{-3}$ |
| Fitting $v_{ref}(t)$ | $1.46 \times 10^{-2}$ | $N$ | 2 | 1 | $7.30 \times 10^{-3}$ |
| Synchronisation | $2.83 \times 10^{-5}$ | $N$ | $\sqrt{6}$ | 1 | $1.16 \times 10^{-5}$ |
| Combined uncertainty | | | | | 0.0075 |

$u_{nc}$ = Uncertainty range
PD = Probability distribution ($N$ = Normal; $T$ = Triangular)
div = Divisor
$c_i$ = Sensitivity coefficient
$u_{std}$ = Contribution to the standard uncertainty

measurements which is necessary to determine their phase difference.

To estimate the uncertainty contribution due to an erroneous synchronisation, a synchronisation test was carried out. To this end, both DMMs have been connected in parallel to a test impedance (see section 4.1). An AC current (2 A) has been impressed on the test impedance. Both DMMs have measured the AC voltage at the same time (40 samples per sine wave, 400 samples corresponding to ten sine waves). Afterwards, the DMMs have been switched and the measurement has been repeated. The uncertainty of the synchronisation has been estimated from the phase differences of the measured AC signals. The synchronisation test has been conducted at different frequencies (1, 10, 100 Hz and 1 kHz) to assess the dependence of the uncertainty on frequency. Additionally, the synchronisation test has been conducted with the reference resistor.

Table 8 shows the results of the synchronisation test for different frequencies of the voltage signal. The results are expressed in terms of the relative phase differences between the corresponding AC sin-voltage curves. The column on the right-hand side of the table shows the relative standard uncertainty $u_{sync}$ assigned to synchronisation errors. The relative phase differences of the reference resistor $R_{ref}$ have higher values than the values of the test impedance, so, $u_{sync}$ values are calculated from the relative phase difference data of $R_{ref}$. They have been estimated from the various results (DMMs switched). The synchronisation error is significantly larger at larger frequencies.

Table 9 summarizes the uncertainty contributions exemplarily for the phase difference measurement of the test impedance at 100 Hz. The major contributions result from fitting $V_{ref}$. The overall combined standard uncertainty of the voltage phase difference is about 0.0327°.

Table 10 indicates the combined uncertainties for the phase difference between $i(t)$ and the $v_{DUT}(t)$ with respect to table 4 for various frequency. It can be seen that the uncertainty increases with increasing frequency.

### 3.3. Reference resistor

The reference resistor has been calibrated by PTB with a DC current. The corresponding uncertainty is shown in table 11.

**Table 10.** Combine uncertainty for the phase difference $\varphi$.

| Freq/Hz | $\varphi$/° | $u(\pi)$/° |
|---|---|---|
| 3162 | 42.790 | 0.046 |
| 1000 | 22.326 | 0.022 |
| 100 | −10.708 | 0.0075 |
| 10 | −15.551 | 0.0036 |
| 1 | −1.8581 | 0.00019 |

**Table 11.** Coaxial shunt calibration.

| Measuring current | Measuring frequency | Resistance $R_{DC}$ | Relative deviation $\partial_R(f)$ | Standard uncertainty |
|---|---|---|---|---|
| 10 A | DC | 80.0092 mΩ | — | 0.55 μΩ |
| 10 A | 10 Hz | — | $-4.5\,\mu\Omega\,\Omega^{-1}$ | $20\,\mu\Omega\,\Omega^{-1}$ |
| 10 A | 100 Hz | — | $-1.0\,\mu\Omega\,\Omega^{-1}$ | $20\,\mu\Omega\,\Omega^{-1}$ |
| 10 A | 1 kHz | — | $-0.3\,\mu\Omega\,\Omega^{-1}$ | $20\,\mu\Omega\,\Omega^{-1}$ |
| 10 A | 10 kHz | — | $-3.7\,\mu\Omega\,\Omega^{-1}$ | $20\,\mu\Omega\,\Omega^{-1}$ |

The main uncertainty contribution results from the frequency-dependence of the resistance value. It is expressed as the relative deviation of the modulus of the measured impedance at frequency $f$ from the calibrated DC value $R_{DC}$:

$$|Z(f)|_{AC} = R_{DC}\,[\partial_R(f) + 1] \tag{13}$$

$$\text{With } \partial_R(f) = \frac{|Z(f)|_{AC} - R_{DC}}{R_{DC}}. \tag{14}$$

Another source of uncertainty is the stability of the device over time between annual calibrations. The approximate 1 year stability is 18 $\mu\Omega\ \Omega^{-1}$ [13]. Thus, the combined standard uncertainty of an 80 mΩ reference resistor is around 2.2 μΩ in the frequency range of interest, if calibration uncertainty at DC, uncertainty of $\partial_R(f)$ and stability are considered.

### 3.4. Contact resistances and wiring

The effect of contact resistances can be neglected due to the four terminal connection with separate voltage and current leads. What is remaining, are erranous voltages, which are induced into the voltage leads due to the mutual inductance between potential and current leads. These can be estimated by a mock up of the current path inside a Li-ion prismatic cell. To achieve this, a dummy cell has been constructed, where the current and voltage paths are realized by separated but running in parallel conductors (see figure 4). The impedance $Z_{dummy}(f)$ is measured replaceing the DUT by this dummy cell. It results mainly from the mutual inductance of the dummy cell and the measurement wires, and can thus be subtracted from the measured impedance results $Z_{DUT\_meas}(f)$ to correct for mutual inductance:

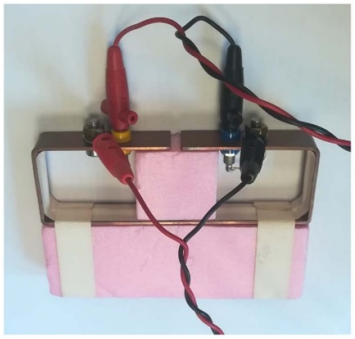

**Figure 4.** Special current loop to mimic the current flow inside a Li-ion prismatic cell. It represents an ideal cell with no resistance but a mutual inductance between potential (center banana jacks) and current (outer bolt terminals) leads.

$$Z_{DUT}(f) = Z_{DUT\_meas}(f) - Z_{dummy}(f). \tag{15}$$

We have also considered an uncertainty contribution $u(Z_{dummy})$ assigned to the correction, which we assume is dominated by the noise of the measurement. The uncertainty of the correction is 0.86 μΩ.

Inductive effects cannot completely be eliminated in the challenging mΩ range and can lead to significant uncertainties of the measured impedances with increasing frequency. The remaining uncertainty contributions due to induction are difficult to be quantified. For the time being, we have limited our investigation to the frequency range where the impedance spectrum of a resistor shows no frequency dependence, assuming that the remaining inductive uncertainty contributions are significantly smaller in that frequency range compared to the other uncertainty contributions. It should be noted that uncertainties due to capacitve stray effects are negligible in the frequency range of interest here.

### 3.5. Frequency

The uncertainties of measured $Z_{DUT}$ values do not explicitly depend on frequency since the terms depending on frequency explicitly cancel in the ratio of equation (7). However, impedances of a specific DUT depend implicitly on frequency through the frequency dependences of the voltage amplitudes and phase differences. Thus, the uncertainty of the fitted sinwave frequency $f_{fit}$ must be calculated and the dependence of the impedance of a specific DUT on frequency must be determined to estimate the effect of frequency uncertainty on the impedance of a specific DUT.

The uncertainty of $f_{fit}$ was determined by progressing the uncertainty of the trigger frequency. To this end, the deviation $\Delta f_{trig\_set}$ of the set value, $f_{trig\_set}$, from the actual frequency of the trigger pulses of the external clock is needed. The actual trigger frequency is given by $f_{trig} = f_{trig\_set} - \Delta f_{trig\_set}$. $\Delta f_{trig\_set}$ was given by the calibration certificate. No uncertainty was assigned to $f_{trig\_set}$ since it is a set value. Using straight forward uncertainty calculation, it can be shown that

**Table 12.** Uncertainty contribution of the frequency to the uncertainty of the impedance.

| $f_{\text{fit}}$/Hz | $f_{\text{trig\_set}}$/Hz | $u_f$ ($\lvert Z_{\text{DUT}}\rvert$)/mΩ |
|---|---|---|
| 3162.23 | 50 596.48 | $1.83 \times 10^{-3}$ |
| 999.991 | 32 000.0 | $5.77 \times 10^{-4}$ |
| 100.0 | 3200 | $5.77 \times 10^{-5}$ |
| 10.0 | 320 | $5.84 \times 10^{-6}$ |
| 1.0 | 32 | $1.07 \times 10^{-6}$ |

**Table 13.** Uncertainty values of the moduli and phases of the test impedance (see section 4.1) at various frequencies.

| Freq | $\lvert Z_{\text{DUT}}\rvert$ | $U(\lvert Z_{\text{DUT}}\rvert)$ | $\varphi$ ($Z_{\text{DUT}}$) | $U_\varphi$ |
|---|---|---|---|---|
| 3162.22 Hz | 2.2671 mΩ | 0.0106 mΩ | 42.79° | 0.092° |
| 999.99 Hz | 1.4914 mΩ | 0.0063 mΩ | 22.33° | 0.043° |
| 316.25 Hz | 1.2950 mΩ | 0.0046 mΩ | 4.921° | 0.008° |
| 100.00 Hz | 1.3506 mΩ | 0.0041 mΩ | −10.71° | 0.015° |
| 31.62 Hz | 1.8790 mΩ | 0.0040 mΩ | −23.46° | 0.022° |
| 10.00 Hz | 2.7312 mΩ | 0.0029 mΩ | −15.55° | 0.0073° |
| 3.98 Hz | 2.9804 mΩ | 0.0013 mΩ | −7.0721° | 0.0016° |
| 1.00 Hz | 3.0392 mΩ | 0.0011 mΩ | −1.8581° | 0.0004° |

the uncertainty $u(f_{\text{fit}})$ of the frequency of the fitted sin-voltages is given by:

$$u(f_{\text{fit}}) = f_{\text{fit}} \frac{u(\Delta f_{\text{tri}_{\text{set}}})}{f_{\text{trig}}}. \tag{16}$$

Note that $f_{\text{fit}}$ is linked to the trigger frequency, since the latter establishes the time axis of the sin-waves (also see figure 2). $u(f_{\text{fit}})/f_{\text{fit}}$ is in the order of $10^{-6}$. It must also be noted that the differences of the fitted frequencies of the current and voltage signals were negligible since both signals were strongly correlated (same circuit, simultaneously measured with the same trigger signal).

Finally, a linear relation $\Delta Z_{\text{DUT}}(f)/\Delta f$ was established piecewise after the measurement of a spectrum. These values were used to estimate the sensitivity coefficients and the uncertainty contribution of the frequency to the uncertainties the impedance:

$$u_f(Z_{\text{DUT}}) = \frac{\Delta Z_{\text{DUT}}(f)}{\Delta f} u(f_{\text{fit}}). \tag{17}$$

This investigation can basically be applied to any representation of $Z_{\text{DUT}}$ (modulus/phase, real/imaginary). Table 12 shows exemplary uncertainty contributions of the frequency to the uncertainty of the modulus of the impedance.

### 3.6. Combined uncertainty of $Z_{DUT}$

The measurement function to calculate $Z_{\text{DUT}}$ is given by equation (7). Thus, assuming an infinite number of degrees of freedom for each uncertainty contribution, the expanded (95%) uncertainty of the modulus of $Z_{\text{DUT}}$ is given by:

$$U_C(|Z_{\text{DUT}}|) = 2\sqrt{\left[u(V_{\text{ref}})\frac{V_{\text{DUT}}R_{\text{ref}}}{(V_{\text{ref}})^2}\right]^2 + \left[u(V_{\text{DUT}})\frac{R_{\text{ref}}}{V_{\text{ref}}}\right]^2 + \left[u(R_{\text{ref}})\frac{V_{\text{DUT}}}{V_{\text{ref}}}\right]^2 + u_f{}^2(|Z_{\text{DUT}}|)}. \tag{18}$$

The expanded uncertainty of the phase difference is given by:

$$U_C(\varphi_{\text{DUT}}) = 2\sqrt{[u(\varphi_{\text{fit}})]^2 + [u(\varphi_{\text{sync}})]^2 + u_f{}^2(|\varphi_{\text{DUT}}|)}. \tag{19}$$

Table 13 shows exemplarily the uncertainties of a passive test impedance at various frequencies. The uncertainty value increases with increasing frequency. At the highest frequency that can be achieved, the impedance uncertainty value is 0.0106 mΩ, or 0.47%, respectively. The test impedance and the measurement results will be discussed in more detail in the next section.

Finally, table 14 shows the individual contributions of the input quanties of equations (18) and (19) to the uncertaint of the $|Z_{\text{DUT}}|$ and $\varphi_{\text{DUT}}$ at selected frequencies. The values correspond to the individual terms of equations (18) and (19). The major contribution to $|Z_{\text{DUT}}|$ results from $u(V_{\text{DUT}})$, which mainly results from fitting. Likewise, the major contribution to $\varphi_{\text{DUT}}$ also results from signal fitting of $V_{\text{DUT}}$. Thus, measures to reduce noise would be a promising means to reduce the uncertainty of the measurement.

## 4. Characterisation of a passive low impedance reference standard

### 4.1. Test impedance

In this section, the characterisation of a passive test impedance is presented. The test impedance is designed such that its impedance spectrum reflects typical features of a low impedance battery cell and can be operated with currents and voltages similar to impedance measurements of high energy cells. It includes a resistor $R2$ to represent the serial resistances of current collectors, electrolyte and contact resistances.

**Table 14.** Uncertainty components of $|Z_{DUT}|$ and $\varphi_{DUT}$, respectively.

| | $u_{xi}(\lvert Z_{DUT}\rvert)$ | | |
|---|---|---|---|
| *xi* | At 1 Hz | At 10 Hz | At 100 Hz |
| $V_{ref}$ | $9.18 \times 10^{-4}$ mΩ | $1.46 \times 10^{-3}$ mΩ | $1.04 \times 10^{-3}$ mΩ |
| $V_{DUT}$ | $6.38 \times 10^{-4}$ mΩ | $2.46 \times 10^{-3}$ mΩ | $4.02 \times 10^{-3}$ mΩ |
| $R_{ref}$ | $2.29 \times 10^{-3}$ mΩ | $2.29 \times 10^{-3}$ mΩ | $2.29 \times 10^{-3}$ mΩ |
| $f$ | $1.07 \times 10^{-6}$ mΩ | $5.84 \times 10^{-6}$ mΩ | $5.77 \times 10^{-5}$ mΩ |
| | $u_{xi}(\varphi_{DUT})$ | | |
| | At 1 Hz | At 10 Hz | At 100 Hz |
| $\varphi_{fit\ Vref}$ | $1.28 \times 10^{-4}$ ° | $1.91 \times 10^{-3}$ ° | $1.90 \times 10^{-3}$ ° |
| $\varphi_{fit\ VDUT}$ | $1.36 \times 10^{-4}$ ° | $3.10 \times 10^{-3}$ ° | $7.30 \times 10^{-3}$ ° |
| $\varphi_{sync}$ | $6.07 \times 10^{-7}$ ° | $1.09 \times 10^{-5}$ ° | $1.16 \times 10^{-5}$ ° |
| $f$ | $1.07 \times 10^{-6}$ ° | $5.84 \times 10^{-6}$ ° | $5.77 \times 10^{-5}$ ° |

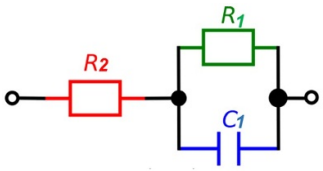


**Figure 5.** Schematic of the test impedance $R2 \approx 1$ mΩ. $R1 \approx 2$ mΩ. $C1 \approx 3.7$ F.

Furthermore, it includes a resistor and a capacitor in parallel, $R_1\|C_1$, approximating the charge transfer resistance and double layer capacitance at the electrode/electrolyte interfaces. Figure 5 shows the schematic diagram of the test impedance and the nominal values of its components.

### 4.2. Characterisation of the test impedance

The test impedance is designed such that its components can be measured individually. Impedance spectra of three configurations have been measured: $R_2$, $R_1\|C_1$ and the total impedance of $R_2 + R_1\|C_1$. The frequency range was from 1 Hz to 3 kHz. Figure 6 shows the measured spectra in terms of the moduli and the phases of the impedances for all three configurations (Bode-plots). Uncertainties are not shown in this figure since they cannot reasonably be resolved on this scale.

The spectra show the expected behaviour qualitatively for each of the configurations up to about 100 Hz, which is indicated by the vertical line. The modulus of $R_2$ is a constant and the corresponding phase is zero. The modulus of the $R1\|C_1$ configuration is $R_1$ at low frequencies and decreases towards zero with increasing high frequencies. The minimum of the phase is around 50 Hz, which does, however, not correspond to the critical frequency $1/R_1C_1 \approx 20$ Hz. At low frequencies, $R_1$ and $R_2$ sum up in the $R_2 + R_1\|C_1$ configuration and approaches $R_2$ at higher frequencies.

The spectra start to show increasing deviations from the expected behaviour above 100 Hz due to inductive contributions. This can particularly be seen in the spectrum of $R_2$ which should be constant over the whole frequency range. Likewise,

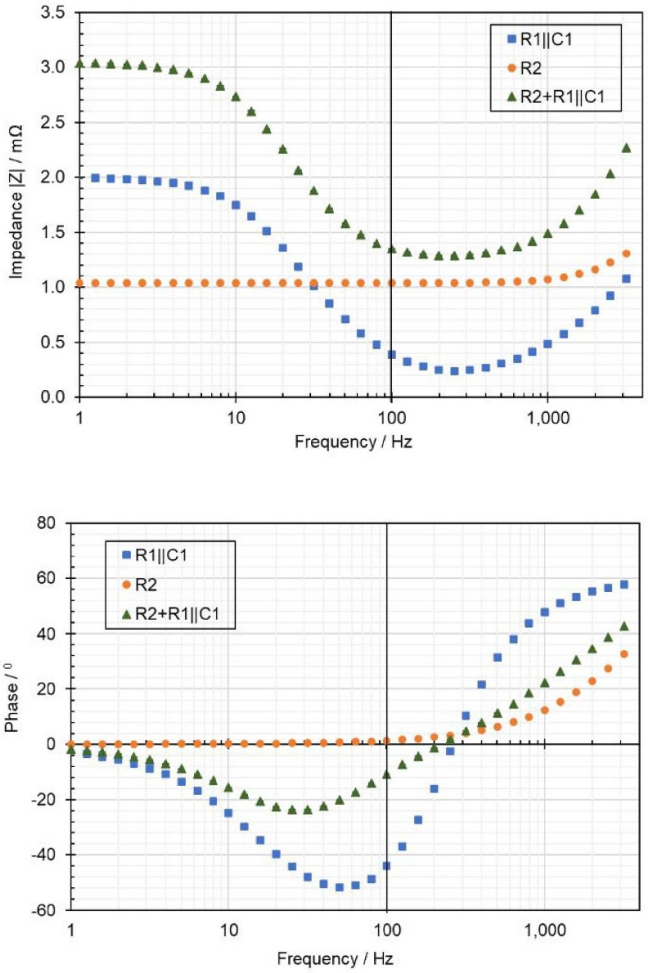


**Figure 6.** Spectra of moduli and phases of the test impedance. The vertical line indicates 100 Hz, above which the spectra are significantly affected by inductive effects.

the $R_2 + R_1\|C_1$ configuration should approach a purely resistive behaviour with zero phase at high frequencies while the $R_1\|C_1$ becomes a pure $C$ at high frequencies with $-90°$ phase. Hence, the simple equivalent circuit shown in figure is not adequate, since we have real components with lead resistances and inductances. In fact, the actual equivalent circuit needs not to be known to characterise the test impedance. Such unknown parasitic impedances can be accepted as a part of the test impedance if they are stable. As we will demonstrate in the next section, there is reasonable evidence that the induction causing the distortion must indeed be associated to the test impedance rather than to the reference spectrometer and the lead wires.

## 5. Comparison with an alternative method

The validation of the reference spectrometer has been performed by comparing the results of the test impedance with the impedance measurement system used in [10] which is based on the measurement of effective voltages and currents.

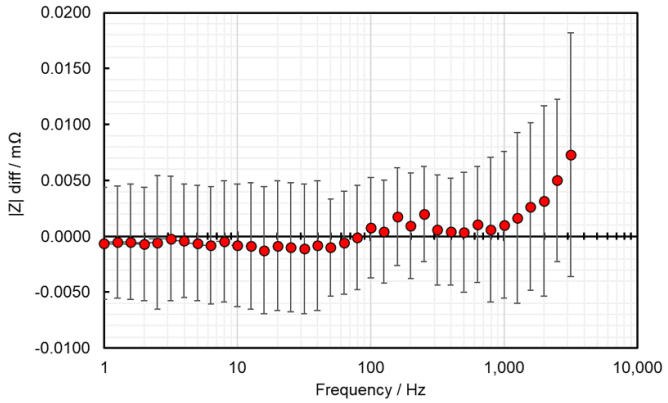


**Figure 7.** Difference of the moduli of the test impedance measured with the reference spectrometer and the effective voltage/current method. The error bars indicate the expanded uncertainty of the difference.

### *5.1. Basic concept of the effective voltage and current measurement procedure*

That measurement procedure impresses a constant AC-current $i(f)$ on the DUT at various frequencies $f$ (1 Hz $\leqslant f \leqslant$ 10 kHz) in a 1–2–5 sequence per decade. The resulting voltage drop is measured with a digital voltmeter, measuring the effective voltage $U_{\mathrm{eff}}$ and the corresponding effective current $I_{\mathrm{eff}}$. The modulus of the impedance $|Z|\,(f)$ is calculated from:

$$|Z|\,(f) = \frac{U_{\mathrm{eff}}\,(f)}{I_{\mathrm{eff}}\,(f)} = \frac{U\,(f)}{I\,(f)}. \tag{20}$$

With $U(f)$ and $I(f)$ being the amplitudes of the corresponding sin-waves. The uncertainty is 0.0049 mΩ. Assuming the measured impedance is that of a known network of passive elements, $|Z(f)|$ can be calculated from the passive elements. Regarding our test impedance (figure 3), $|Z(f)|$ can be calculated from $R_2$. $R_1$ and $C_1$ with equation (20), with $\omega$ being the angular frequency $2\pi f$:

$$|Z(f)| = \sqrt{\left(R_2 + \frac{R_1}{1+\omega^2 R_1^2 C_1^2}\right)^2 + \omega^2\left(\frac{R_1^2 C_1}{1+\omega^2 R_1^2 C_1^2}\right)^2}. \tag{21}$$

Using equation (21), $|Z(f)|$ can be fitted into the measured values to get the values for $R_2$, $R_1$ and $C_1$.

### *5.2. Comparison results*

Both methods, the impedance spectrometer described above and the effective voltage/current method, have been used to measure the test impedance (figure 5). The results are presented in the figure 7. It shows a plot of the differences of $|Z(f)|$ of the $R_2 + R_1 \| C_1$ configuration versus frequency. The uncertainty bars indicate the uncertainty of the difference:

$$U\left(\Delta\,|Z(f)|\right) = \sqrt{U_1^2\left(|Z(f)|\right) + U_2^2\left(|Z(f)|\right)}. \tag{22}$$

$U_1$ and $U_2$ are the expanded uncertainties of both methods.

It can be seen that both methods provide consistent results up to 1 kHz. Thus, it can be reasonably assumed that the inductive effects distorting the measured impedances in figure 4 must be a property of the test impedance and that the reference spectrometer provides reliable impedance spectra at least up to 1 kHz.

### *5.3. Evaluation*

Both methods can be used to characterise the spectrum of the moduli of a passive impedance standard that has to be characterised as a primary reference for impedance spectrometers. However, the effective voltage/current methods can only be used to provide correct phase information for such a impedance standard if parasitic impedances can be neglected and the assumed equivalent circuit is adequate. Otherwise, as in the present case, the derived values for the circuit elements are erroneous. Therefore, it must be assumed that the value of $C_1$ shown in figure 5, which results from the application of the effective voltage and current measurement procedure, is erroneous. This also explains the deviation of the calculated critical frequency and that derived from figure 6. The presented reference spectrometer overcomes this problem, since a measured impedance spectrum (i.e. moduli and phases) does not require specific knowledge of the circuitry of the impedance standard. In fact, parasitic effects can be accepted as long as they are part of the impedance standard and do not change over time.

## 6. Summary and outlook

We have presented a reference spectrometer that can be used as a primary measurement method to characterise impedance standards in the low mΩ range with AC currents of a few Amps and up to one kHz. These operation parameters are most relevant for electrochemical impedance spectroscopy of high energy Li-ion cells, which are used for electric vehicles. We have further presented a comprehensive uncertainty budget of respective impedance measurements. The expanded uncertainty (95% coverage level) of the modulus increases from around 1 to 6 μΩ, and that of the phase from around 0.001° to 0.1° between 1 Hz and 1 kHz. The major contributions to the uncertainty of both quantities result from fitting the sin-signals. Measures to reduce noise could decrease the uncertainty. The spectrometer showed good equivalence up to 1 kHz when compared with an alternative method, that is based on effective voltage and current measurements. It is however better suited to assign correct phases to the test impedance.

Currently, the spectrometer can only be applied to passive reference resistances that have no voltage bias. However, impedance spectroscopy of Li-ion cells necessarily includes the application of an adequate voltage bias to compensate the cell voltage. Therefore, impedance standards should also include a voltage bias for appropriate impedance meter calibration. The reference spectrometer will be developed further in a future project to be applicable to respective impedance standards.

## Data availability statement

The data that support the findings of this study are available upon reasonable request from the authors.

## Acknowledgments

This work has been carried out as part the project 17IND10 'LiBforSecUse' that has received funding from the EMPIR programme co-financed by the Participating States and from the European Union's Horizon 2020 research and innovation programme. We gratefully acknowledge the support of the Braunschweig International Graduate School of Metrology B-IGSM.

## ORCID iDs

Benyamin H Rusanto https://orcid.org/0000-0003-2530-1873
Steffen Seitz https://orcid.org/0000-0003-4702-0001

## References

[1] Medding N *et al* Applications of electrochemical impedance spectroscopy to commercial Li-ion cells *J. Power Sources* **480** 228742
[2] BIPM. IEC. IFCC. LAC. IUPAC. IUPAP. ISO. OIMLl 2012 The international vocabulary of metrology—basic and general concepts and associated terms (VIM) (available at: www.bipm.org/utils/common/documents/jcgm/JCGM_200_2012.pdf)
[3] LiBforSecUse Quality assessment of electric vehicle Li ion batteries for second use applications (available at: www.ptb.de/empir2018/libforsecuse/home/)
[4] Callegaro L, D'Elia V, Kampik M, Kim D B, Ortolano M and Pourdanesh F 2015 Experiences with a two-terminal-pair digital impedance bridge *IEEE Trans. Instrum. Meas.* **64** 1460–5
[5] Callegaro L, D'Elia V, Ortolano M and Pourdanesh F 2015 A three-arm current comparator bridge for impedance comparisons over the complex plane *IEEE Trans. Instrum. Meas.* **64** 1466–71
[6] Overney F, Flowers-Jacobs N E, Jeanneret B, Rüfenacht A, Fox A E, Underwood J M, Koffman A D and Benz S P 2016 Josephson-based full digital bridge for high-accuracy impedance comparisons *Metrologia* **53** 1045–53
[7] Maslan S, Síra M, Skalick T and Bergsten A T 2019 Four-terminal pair digital sampling impedance bridge up to 1 MHz *IEEE Trans. Instrum. Meas.* **68** 1860–9
[8] Palafox L, Raso F, Ku J, Overney F, Callegaro L, Gournay P, Zio A, Nissil J, Eklund A G and Lippert T 2013 AIM QuTE: automated impedance metrology extending the quantum toolbox for electricity *16th Int. Congress of Metrology 11001* pp 1–3
[9] Overney F and Jeanneret B 2017 Calibration of an LCR-meter at arbitrary phase angles using a fully automated impedance simulator *IEEE Trans. Instrum. Meas.* **66** 1516–23
[10] Funck T, Eberhardt R, Heine J, Bastkowski F and Spitzer P 2014 Calibration of EIS analyzers using reference impedances *17th ITG/GMA Symp. on Sensor and Measuring Systems* (*Nürnberg*, *3–4 June 2014*)
[11] Maslan S 2020 Design of digital sampling impedance bridge for battery impedance spectroscopy*IMEKO TC4 Int. Symp.* (https://doi.org/10.5281/zenodo.4630641)
[12] Ramos P M *et al* 2015 Evaluation of the uncertainty of electrical impedance measurement: the GUM and it's supplement 2 *J. Phys.: Conf. Ser.* **588** 012045
[13] Fluke 2015 A40B precision AC current shunt set instruction *Manual Rev.* **2** 21
[14] Espel P, Poletaeff A and Bounouh A 2009 Characterisation of analogue-to digital converters of a commercial digital voltmeter in the 20 Hz to 400 Hz frequency range *Metrologia* **46** 578–84
[15] Rydler K-E, Svensson S and Tarasso V 2002 Voltage dividers with low phase angle errors for a wideband power measuring system *Conf. Dig. CPEM* pp 382–3
[16] Svensson S, Rydler K-E and Tarasso V 2004 Improved model and phase angle verification of current shunts for AC and power measurements *Conf. Digest CPEM* pp 82–83
[17] IEEE Std. 1057 1993 Standard for digitizing waveform records
[18] JCGM 100:2008 Evaluation of measurement data—guide to tht expression of uncertainty in measurement (available at: www.bipm.org/documents/20126/2071204/JCGM_100_2008_E.pdf/cb0ef43f-baa5-11cf-3f85-4dcd86f77bd6)
[19] Keysight 2014 *Multimeter: Shattering performance barriers of speed and accuracy* (Santa Rosa, CA: Keysight Technologies)
[20] Krajewski M 2018 Constructing an uncertainty budget for voltage RMS measurement with a sampling voltmeter *Metrologia* **55** 95–105